

Bridging Geometry and Appearance: Topological Features for Robust Self-Supervised Segmentation

Haotang Li¹ Zhenyu Qi¹ Hao Qin² Huanrui Yang¹ Sen He¹ Kebin Peng³

¹ Department of Electrical and Computer Engineering, The University of Arizona, Tucson, AZ, USA

² Department of Mathematics, The University of Arizona, Tucson, AZ, USA

³ Department of Computer Science, East Carolina University, Greenville, NC, USA

Abstract

*Self-supervised semantic segmentation methods often fail when faced with appearance ambiguities. We argue that this is due to an over-reliance on unstable, appearance-based features such as shadows, glare, and local textures. We propose **GASeG**, a novel framework that bridges appearance and geometry by leveraging stable topological information. The core of our method is Differentiable Box-Counting (**DBC**) module, which quantifies multi-scale topological statistics from two parallel streams: geometric-based features and appearance-based features. To force the model to learn these stable structural representations, we introduce Topological Augmentation (**TopoAug**), an adversarial strategy that simulates real-world ambiguities by applying morphological operators to the input images. A multi-objective loss, **GAloss**, then explicitly enforces cross-modal alignment between geometric-based and appearance-based features. Extensive experiments demonstrate that GASeG achieves state-of-the-art performance on four benchmarks, including COCO-Stuff, Cityscapes, and PASCAL, validating our approach of bridging geometry and appearance via topological information.*

1. Introduction

Self-supervised semantic segmentation addresses the fundamental challenge of partitioning an image into semantically meaningful regions without specialized annotations [16]. This capability is crucial for various applications, including autonomous driving [41], industrial inspection [37], and geographic data analysis [50], where obtaining dense annotations is often impractical or infeasible.

Most SOTA methods primarily focused on learning more appearance-based features, such as shared color and texture [6]. However, these methods struggle when faced with appearance ambiguities, where semantically distinct objects exhibit similar visual features, due to their over-reliance on

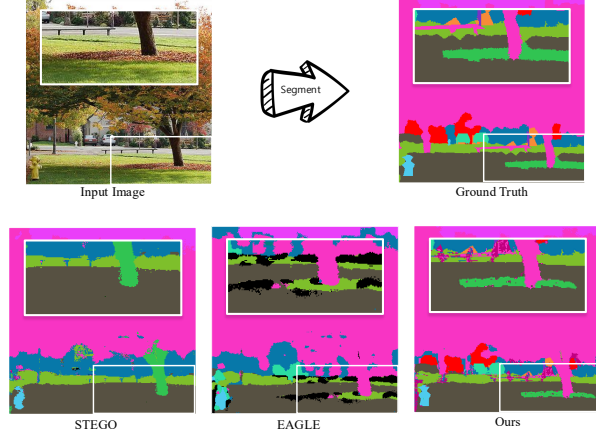


Figure 1. Qualitative comparison of semantic segmentation results on an image from the COCO-Stuff dataset. Our method (GASeG) successfully disambiguates the tree trunk and leaves from the background, overcoming appearance ambiguities (e.g., shadows, textures) that cause segmentation failures in state-of-the-art methods like STEGO and EAGLE.

these appearance cues [8]. To tackle this challenge, recent works incorporate extra information to achieve a more reliable segmentation, such as infrared images [28], lidar data [3], and depth maps [38]. While these approaches show improvements, they still overlook a more fundamental element: topological information.

Motivated by this, we introduce **GASeG**(Geometry and Appearance aware Self-Supervised Segmentation), a novel framework that leverages topological information to bridge geometry and appearance cues for accurate segmentation. Specifically, topological information bridges geometry-based features and appearance-based features, which capture stable properties such as connectivity, holes, and boundaries. These properties remain invariant under continuous deformations [26], such as stretching or bending, enhancing GASeG’s robustness.

GASeG relies on three core components to bridge geom-

etry and appearance. The framework begins with Topological Augmentation (**TopoAug**), an adversarial strategy that applies morphological operators to the luminance channel to prevent the model from taking "shortcuts" by learning unstable features. Consequently, the model is forced to rely on stable ones extracted by our Differentiable Box-Counting module (**DBC**). This module quantifies the multi-scale fractal complexity of (i) geometric-based features from depth maps, and (ii) appearance-based features from frozen image encoder. Finally, we design a multi-objective loss function (**GALoss**) to regularize the training process, explicitly enforcing cross-modal alignment between these geometric and semantic representations.

Figure 1 highlights the performance of GASEg under appearance ambiguity. While SOTA methods fail to clearly segment the leaves or produce fragmented masks due to similar textures, GASEg accurately delineates fine-grained boundaries, yielding a cohesive result that closely matches the Ground Truth.

Our main contributions are as follows:

1. We propose GASEg, a novel framework for self-supervised semantic segmentation that leverages topological information to bridge geometry and appearance, thereby enhancing accuracy.
2. We introduce Topological Augmentation to force learning stable features from Differentiable Box-Counting Module, and GALoss to enforce geometric consistency. Together, these components provide topological guidance against appearance ambiguities.
3. We empirically demonstrate that GASEg achieves state-of-the-art accuracy across four benchmarks (COCO-Stuff, Cityscapes, Potsdam, and PASCAL), and comprehensive ablation studies validate each component.

2. Related Work

Semantic Segmentation: Following the success of self-supervised vision transformers like DINO [5], a dominant paradigm has emerged: freezing the pre-trained backbone and training lightweight, task-specific segmentation heads. For example, Seitzer *et al.* [33] build the feature maps with slot attention from different slots. Seong *et al.* [35] build the feature maps by discovering hidden positives from task-agnostic and task-specific feature pools. Li *et al.* [22] encode concepts into learnable prototypes for pixel-level semantic aggregation in self-supervised vision transformer pre-trained models for segmentation. CAUSE [21] bridges an intervention-oriented approach to define suitable two-step tasks for unsupervised prediction. U2Seg [30] generates pseudo-semantics clustering labels used for self-training segmentation tasks. EAGLE [20] introduces EiCue to provide semantic and structural cues through eigen vectors derived from the semantic similarity matrix of image features and color affinity from images.

Topological Tools in Image Processing: In the literature, early image processing works use topological tools. For example, Wu *et al.* [43] propose Deep Closing that uses a classic closing operation to generate the Masked Image Modeling paradigm to enhance topology knowledge. Berger *et al.* [1] use a loss function to measure the confidence level of topological information across multi-class segmentation. Xu *et al.* [45] learn to minimize a topological error from unlabeled images and integrates it into the loss function. Wang *et al.* [42] use Tree Segmentation in CT Scans. Yao *et al.* [47] use a topology-aware deep learning-based approach in identifying cancer areas. Shen *et al.* [36] use topological errors for vessel segmentation. Mahrous *et al.* [27] use topological segmentation in three-dimensional vector fields. Fu *et al.* [11] use topology reasoning for lane detection in autonomous driving. Hu *et al.* [17] use a continuous-valued loss function to decrease topological errors on fine-scale structures. Liu *et al.* [23] use topology for point clouds.

3. GASEg

3.1. Overall Framework

To bridge geometry and appearance, we propose GASEg, which is illustrated in Figure 2. Starting with an input image, we learn two patterns by using different feature extraction paths. For the first path, to prepare the feature extraction, we use a frozen image encoder at the top to extract pixel-level representations. Then, we use Pseudo Head and frozen depth estimator to extract the depth maps and pseudo embeddings, respectively. We apply the prototypical clustering on the embedding to generate the pseudo labels. After that, for each kind of depth map and pseudo labels, we extract the topological features by the Differentiable Box-Counting Module. In our approach, we use the soft-box-counting method described in Section 3.2 to extract multi-scale topological information.

Simultaneously, the input image to the second path is augmented by a Topological Augmentation module described in Section 3.3 to produce a structurally-corrupted version, which is then passed to the segmentation head (Seg Head). The Seg Head learns to fuse the corrupted appearance features with the stable structural features from DBC, producing the final segmentation output.

The entire framework is trained in a self-supervised manner, to jointly optimize the framework, we introduce a multi-objective loss function GALoss in Sec. 3.4 that computes distinct objectives from the outputs of our core modules, providing targeted supervision for each.

At inference time, we discard the DBC branch and only use the trained Seg Head on the feature representation of input, followed by clustering and DenseCRF post-processing step to obtain the segmentation result.

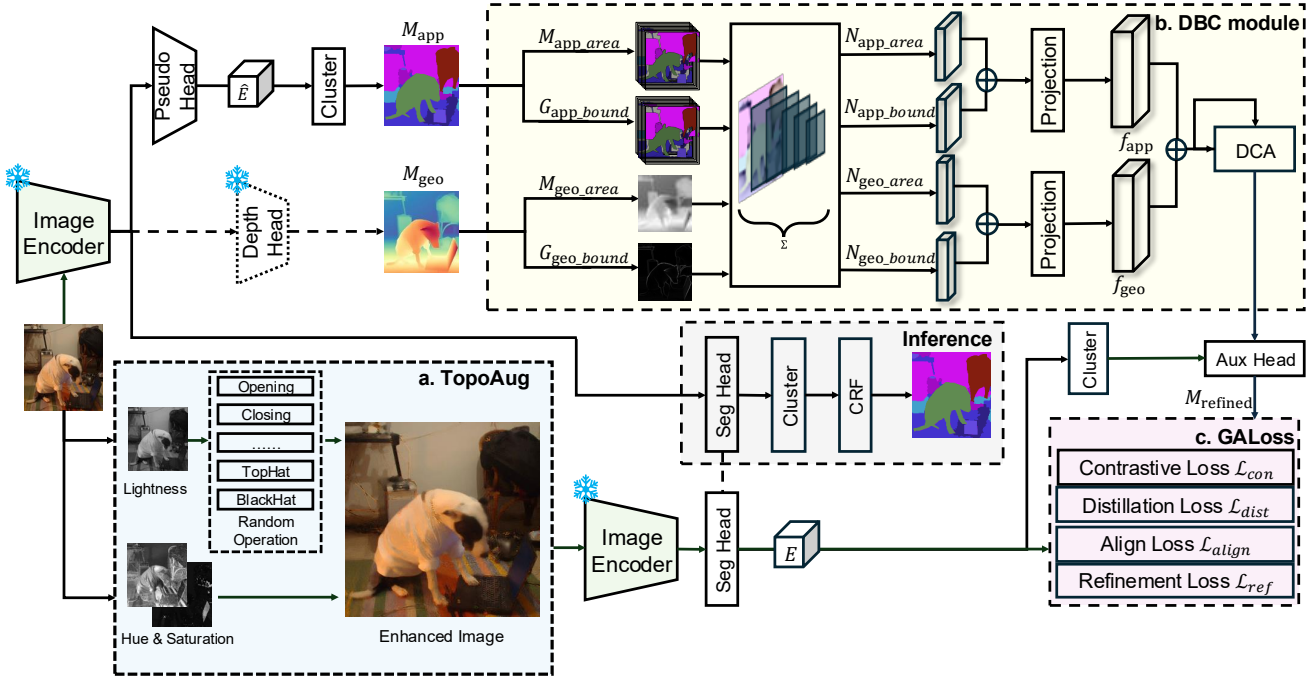


Figure 2. The overall architecture of the GASEG framework. The diagram illustrates both the training and inference pipelines, highlighting the three core components: (a) the Topological Augmentation module, (b) the Differentiable Box-Counting module for learning and bridging geometric and appearance priors, and (c) the multi-objective GALoss function.

3.2. Differentiable Box-Counting Module

The box-counting method is a topology technique that quantifies the topological complexity of a set by measuring how its spatial occupancy scales across multiple resolutions. The original box-counting method is non-differentiable due to its reliance on indicator functions, making it unsuitable for end-to-end training in deep learning frameworks. To overcome this limitation, we introduce the Differentiable Box-Counting Module, which is a gradient-friendly component to extract the soft-box-counting statistics from both appearance and geometric domains.

Box-Counting takes a feature map $M \in \mathbb{R}^{B \times C \times H \times W}$ and a box size s as inputs, and outputs a count of the number of boxes of size s that "occupy" the set represented by M . H and W are the height and width of the map, B is the batch size, and C is the number of channels. We denote the standard box-counting as $BC(s)$ which is defined as:

$$\text{BC}(M, s) := \sum_{i,j} \mathbb{I} \left(\sup_{x \in B_{ij}(s)} \text{MaxPool}(x) > 0 \right)$$

where $B_s(i, j)$ is the (i, j) -th spatial box of dividing the map into non-overlapping boxes of size s . \mathbb{I} is the indicator function. $\text{MaxPool}(x)$ is the max-pooling operation within the box. The standard box-counting $\text{BC}(M, s)$ counts the number of boxes where the maximum value within the box is greater than zero. However, since the indicator function is non-differentiable, the standard box-counting cannot be di-

rectly integrated into a neural network for end-to-end training. To make the box-counting differentiable, we remove the indicator function and use the occupancy signal from map M directly. This modification allows gradients to flow. We denote this new differentiable box-counting as $\text{DBC}(\cdot)$, which is defined as

$$\text{DBC}(M, s) \coloneqq \sum_{i,j} \sup_{x \in B_{ij}(s)} \text{MaxPool}(x)$$

To capture multi-scale topological statistics, we extend the $\text{DBC}(\cdot)$ operator to accept a set of box sizes $S = \{s_1, s_2, \dots, s_k\}$ and output the counts across all scales. Formally, the multi-scale DBC operator is defined as:

$$\text{DBC}(M, \mathbf{S}) \coloneqq \left(\sum_{i,j} \sup_{x \in B_s(i,j)} \text{MaxPool}(x) \right)_{s=1}^k$$

DBC captures the topological complexity of the input map M across multiple resolutions, and is compatible with gradient-based optimization. Additionally, DBC extracts two complementary types of topological information from both the appearance and geometric domains, which are detailed below:

Appearance Domain Extracting robust appearance structure is critical for overcoming appearance ambiguity in self-supervised segmentation. We use a pseudo-label map $M_{\text{pseudo}} \in \mathbb{R}^{B \times H \times W}$ generated by a prototypical clustering

module attached by two complementary encoding methods: area counting and boundary counting.

The area counting captures the spatial dispersion of class regions, while the boundary counting captures the complexity of class boundaries. We use one-hot encoding to convert the pseudo-label map into a binary mask $M_{\text{app}} \in \{0, 1\}^{B \times C \times H \times W}$ and apply the DBC operator to extract multi-scale topological statistics. This yields the appearance area counting tensor $N_{\text{app}, \text{area}} \in \mathbb{N}^{B \times C \times k}$:

$$N_{\text{app}, \text{area}} = \text{DBC}(M_{\text{app}}, S)$$

To measure boundary complexity, instead of using the raw mask M_{app} , we isolate the class boundaries by computing the full, symmetric Morphological Gradient (the difference between dilation and erosion) to obtain a gradient map G_{seg} , and then apply DBC to G_{seg} to compute the appearance boundary counting $N_{\text{app}, \text{bound}} \in \mathbb{R}^{B \times C \times k}$:

$$N_{\text{app}, \text{bound}} = \text{DBC}(\text{Dilation}(G_{\text{seg}}) - \text{Erosion}(G_{\text{seg}}), S)$$

Therefore, we obtain two counting tensors from the appearance domain: the area counting $N_{\text{app}, \text{area}}$ and the boundary counting $N_{\text{app}, \text{bound}}$, which together capture the complete topological statistics for this domain.

Geometric Domain We also extract robust geometric structure to complement the appearance features. In the geometric domain, we utilize depth information, which is inherently including geometric cues since depth is relatively invariant to appearance changes of objects. We extract such topological information from a normalized geometric feature map, $M_{\text{geo}} \in \mathbb{R}^{B \times H \times W}$. Similar to the appearance domain, we compute two parallel counting operators: geometric roughness (area counting) and geometric edges (boundary counting).

The geometric roughness captures the local surface complexity (e.g., a "cobblestone road" vs. a "smooth wall"), while the geometric edges isolate primary object contours and depth discontinuities. Let $\mathbb{E}_{3 \times 3}[\cdot]$ denote the local expectation operator, which computes the mean value within a 3×3 sliding window. To estimate the geometric roughness, we compute a local variance map $M_{\text{geo}, \text{area}} \in \mathbb{R}^{B \times 1 \times H \times W}$, which is defined as:

$M_{\text{geo}, \text{area}} = \mathbb{E}_{3 \times 3}[M_{\text{geo}} \circ M_{\text{geo}}] - \mathbb{E}_{3 \times 3}[M_{\text{geo}}] \circ \mathbb{E}_{3 \times 3}[M_{\text{geo}}]$ where \circ denotes element-wise multiplication. We then apply DBC operator to $M_{\text{geo}, \text{area}}$ to quantify its multi-scale composition to obtain the geometric roughness tensor $N_{\text{geo}, \text{area}} = \text{DBC}(M_{\text{geo}}, S)$.

To measure geometric edges, we isolates the scene's primary object contours and depth discontinuities, then compute the gradient magnitude map G_{geo} using a standard Sobel filter. Next, we apply the DBC operator to G_{geo} to compute the geometric edge counting tensor $N_{\text{geo}, \text{bound}} = \text{DBC}(G_{\text{geo}}, S)$. These two tensors capture the complete geometric statistics of geometric domain.

Projection After obtaining the four counting tensors from both appearance and geometric domains at area level and boundary level, we transform them into a latent representation. Appearance tensors $N_{\text{app}, \text{area}}$ and $N_{\text{app}, \text{bound}}$ are concatenated together and projected to a fixed-dimensional appearance feature vector $f_{\text{app}} \in \mathbb{R}^{B \times D_{\text{feat}}}$ through a projection head (Multi-layer Perceptron). Similarly, geometric tensors $N_{\text{geo}, \text{area}}$ and $N_{\text{geo}, \text{bound}}$ are concatenated and projected to a fixed-dimensional geometric feature vector $f_{\text{geo}} \in \mathbb{R}^{B \times D_{\text{feat}}}$ through a different projection head. Notably, we employ two independent, lightweight projection heads. This decoupled projection is a deliberate design choice to make the model to specialize in processing the distinct properties of each domain.

These projected feature vectors f_{app} and f_{geo} capture the multi-scale topological statistics from their respective domains. We concatenate f_{app} and f_{geo} to form the combined feature vector $f_{\text{dbc}} = [f_{\text{app}}; f_{\text{geo}}] \in \mathbb{R}^{B \times 2D_{\text{feat}}}$ and pass it to the Deformable Cross Attention [44] to fuse with the feature from image encoder.

3.3. Topological Augmentation

Data augmentation is widely used in self-supervised segmentation to train a model that is robust to a wide spectrum of real-world visual corruptions. Standard techniques, such as ColorJitter, GaussianBlur, and RandomFlipping, are effective at simulating photometric variations, e.g. changes in lighting and color, and simple geometric transformations. However, these methods fail to simulate a more complex and pernicious class of artifacts: local structural corruptions, such as the non-linear, shape-altering effects of hard shadows or specular glare, which are topological in nature. To bridge this critical gap, we introduce Topological Augmentation, a new augmentation strategy designed to adversarially simulate these artifacts, forcing the model to discard these spurious local cues.

To achieve this, we leverage a set of tools \mathcal{T} from mathematical morphology, which operate on a grayscale intensity function $f(x)$ using a structuring element B . First, we introduce Grayscale Erosion $(f \ominus b)(x) = \inf_{y \in B} [f(x+y) - b(y)]$ and Dilation $(f \oplus b)(x) = \sup_{y \in B} [f(y) + b(x-y)]$, the non-linear operators that simulates the topological effect of hard shadows / specular glare or over-exposure. By composing these two fundamental operators, we derive a richer set of compound transformations: Grayscale Opening $f \circ b = (f \ominus b) \oplus b$, is a filter that breaks thin "bridges" and smooths contours by removing small, bright "peak" artifacts. Grayscale Closing $f \bullet b = (f \oplus b) \ominus b$, is used to fuse narrow breaks and fill small, dark "valley" artifacts, such as micro-shadows. The White Top-Hat $T_w(f) = f - f \circ b$, which isolates bright features to simulate glare. The Black Top-Hat $T_b(f) = f \bullet b - f$, isolates dark features to simulate shadows.

Having defined morphological operator toolbox \mathcal{T} , a naïve approach is to apply directly to each of the RGB channels of image, respectively. However, this will breaks the physical co-variance, destroy the intrinsic color ratios that define an object’s appearance and introduce severe, non-realistic color artifacts [39]. To simulate lighting-based corruptions, decouple the image’s illumination (Lightness) from its chrominance (Color) is more effective [49]. Therefore, we convert the input image from RGB to the HSL color space to isolate the Lightness (L) channel.

To prevent the model from overfitting to any single type of artifact, we set every operator in our toolbox \mathcal{T} to have a non-zero probability factor of being used. After an operator T is selected, its parameters are also randomized: the structuring element B is randomly assigned a size (e.g., 3×3 or 5×5). These randomized operations are applied exclusively to the L-channel. this augmented L-channel is then recombinied with the original H and S channels, converted back to RGB and fed to the network. It simulates the desired topological artifacts (shadows and glare) while preserving the semantic-bearing Hue (H) and Saturation (S) channels completely unaltered. This process generates a vast and unpredictable range of local structural corruptions, effectively simulating the “noise” of real-world shadows and glare.

3.4. Loss Function

To regularize the training process of GASEG, we design a multi-objective loss function, GALoss, note as \mathcal{L}_{GA} . To ensure the Seg Head learns a robust and well-structured feature space, we first apply a pixel-prototype contrastive loss, \mathcal{L}_{con} , which defined by an InfoNCE [31] objective. \mathcal{L}_{con} pulls each pixel feature \mathbf{e}_i from the embedding-level output \mathbf{E} of Seg Head, towards its corresponding class prototype $\hat{\mathbf{e}}_i$ from Pseudo Head’s output $\hat{\mathbf{E}}$, while pushing it away from all other class prototypes $\{\hat{\mathbf{e}}_j\}_{j \neq i}$.

$$\mathcal{L}_{\text{con}} = -\mathbb{E}_i \left[\log \left(\frac{\exp(\text{sim}(\mathbf{e}_i, \hat{\mathbf{e}}_i)/\tau)}{\sum_{j=1}^N \exp(\text{sim}(\mathbf{e}_i, \hat{\mathbf{e}}_j)/\tau)} \right) \right]$$

where $\text{sim}(\cdot, \cdot)$ is the cosine similarity function, τ is a temperature hyperparameter, and N is the total number of class prototypes. This objective ensures the feature space itself is compact and separable, which is critical for robustness against the TopoAug corruptions.

Second, after establishing a robust feature space, we apply a distillation loss, $\mathcal{L}_{\text{dist}}$, to map these strong features to the correct semantic class labels in probability space. This objective operates on the probability map P_{seg} , forcing it to match the one-hot pseudo-label M_{pseudo} , where $P_{\text{seg}} = \sigma(\phi(\mathbf{E}))$ is the softmax $\sigma(\cdot)$ probabilities of projection layer $\phi(\cdot)$ output of Seg Head’s embeddings \mathbf{E} . We use cross-entropy loss, treating the pseudo label M_{pseudo} as a fixed target using stop-gradient $\text{sg}(\cdot)$:

$$\mathcal{L}_{\text{dist}} = -\mathbb{E}_{(h,w)} \left[\sum_{c=1}^C \text{sg}(M_{\text{pseudo}}) \log(P_{\text{seg}}) \right]$$

This objective ensures the final classification $\phi(\mathbf{E})$ is semantically accurate by forcing it to match the stable, uncorrupted pseudo labels (M_{pseudo}) when learning from the topologically-corrupted input.

Next, to ensure the aux labels M_{aux} are geometrically consistent and robust to appearance ambiguity, we apply a cross-modal structure alignment loss, $\mathcal{L}_{\text{align}}$, which calculates the cosine similarity between the appearance structure vector f_{app} and the geometric structure vector f_{geo} .

$$\mathcal{L}_{\text{align}} = 1 - \frac{f_{\text{app}} \cdot f_{\text{geo}}}{\|f_{\text{app}}\|_2 \cdot \|f_{\text{geo}}\|_2}$$

This part of loss forces the learned appearance structure vector f_{app} to align with the geometric structure vector f_{geo} .

Finally, to ensure the auxiliary pathway (DCA, Aux Head) learns to correctly fuse high-resolution DINO features with our topological features (f_{app} , f_{geo}), and apply them correctly on Seg Head, we apply a refinement loss, \mathcal{L}_{ref} , using the multi-class Dice Loss [29], which robustly quantifies the spatial overlap between the pathway’s predicted refinement (M_{aux}) and M_{seg} .

$$\mathcal{L}_{\text{ref}} = 1 - \frac{1}{C} \sum_{c=1}^C \frac{2 \sum_i M_{\text{seg}}^{(c,i)} \cdot M_{\text{aux}}^{(c,i)} + \epsilon}{\sum_i M_{\text{seg}}^{(c,i)} + \sum_i M_{\text{aux}}^{(c,i)} + \epsilon}$$

where C is the number of categories, ϵ is a small constant to avoid division by zero. This loss make Seg Head’s output M_{seg} closer to topological-fused auxiliary head’s output M_{aux} . Meanwhile, the losses applied above will regularized the Seg Head on a right direction.

$$\mathcal{L}_{\text{GA}} = \lambda_{\text{con}} \mathcal{L}_{\text{con}} + \lambda_{\text{dist}} \mathcal{L}_{\text{dist}} + \lambda_{\text{align}} \mathcal{L}_{\text{align}} + \lambda_{\text{ref}} \mathcal{L}_{\text{ref}}$$

Overall, GALoss, presented in Section 3.4, where λ s are the weighting coefficients, decouples the problem by using $\mathcal{L}_{\text{align}}$ and \mathcal{L}_{ref} to solve for appearance ambiguity on the DBC module, creating a stable, high-quality, and topologically-fused target. It also uses a dual-objective $\mathcal{L}_{\text{con}}, \mathcal{L}_{\text{dist}}$ to ensure the Seg Head learns both a robust feature space (critical against TopoAug) and precise classification. Through optimizing this multi-objective function, the framework finally learns to produce segmentation that is both robust to appearance ambiguity and geometrically consistent.

4. Evaluation

4.1. Experiment Setup

Implementation Details We use DINO [32] pretrained vision transformers (ViT-S/8) as our baseline Image Encoder, which keep frozen during training process following prior work [13, 20], a frozen depth estimator pretrained on DINO [46] is used to provide geometric prior. The training images are resized and randomly cropped to 224×224 .

Table 1. Quantitative comparison with SOTA self-supervised segmentation methods across four standard benchmarks: COCO-Stuff, Cityscapes, Potsdam, and PASCAL VOC. Results are reported for both ViT-S/8 and ViT-B/8 backbones using pixel accuracy (Acc) and mean Intersection over Union (mIoU). Our method (Ours) achieves superior performance across all datasets and backbone configurations.

Method	Backbone	Year	COCO-Stuff		Cityscapes		Potsdam		PASCAL
			Acc	mIoU	Acc	mIoU	Acc	mIoU	VOC
CC [18]	VGG11	2015	-	-	63.9	-	63.9	-	-
DeepCluster [4]	VGG11	2018	32.2	9.8	40.7	7.1	41.7	-	42.2
IIC [19]	R18+FPN	2019	21.8	6.7	47.9	6.4	65.1	-	9.8
PiCiE [6]	R18+FPN	2021	48.1	13.8	65.5	12.3	-	-	-
MaskDistill [40]	M R-CNN	2022	-	14.6	-	-	-	-	48.9
DINO [32]	ViT-S/8	2022	28.7	11.3	34.5	10.9	56.6	33.6	-
STEGO [13]	ViT-S/8	2022	48.3	24.5	-	-	-	-	-
TransFGU [48]	ViT-S/8	2022	52.7	17.5	77.9	16.8	-	-	37.2
ACSeg [22]	ViT-S/8	2023	-	16.4	-	-	-	-	47.1
HP [34]	ViT-S/8	2023	54.5	24.3	80.1	18.4	-	-	-
PriMaPs [12]	ViT-S/8	2024	46.5	16.4	81.2	19.4	62.5	38.9	-
DepthG [38]	ViT-S/8	2024	55.1	26.7	-	-	80.4	-	-
EAGLE [20]	ViT-S/8	2024	64.2	27.2	81.8	19.7	-	-	-
Ours	ViT-S/8	66.5	28.9	83.1	21.5	83.1	67.3	54.9	
DINO [32]	ViT-B/8	2022	30.5	9.6	43.6	11.8	66.1	49.4	-
STEGO [13]	ViT-B/8	2022	56.9	28.2	73.2	21.0	77.0	62.6	-
HP [34]	ViT-B/8	2023	-	-	79.5	18.4	82.4	68.6	-
PriMaPs [12]	ViT-B/8	2024	48.5	21.9	59.6	17.6	80.5	67.0	-
EAGLE [20]	ViT-B/8	2024	-	-	79.4	22.1	83.3	71.1	-
DepthG [38]	ViT-B/8	2024	58.6	29.0	81.6	23.1	-	-	-
Ours	ViT-B/8	68.0	30.1	85.7	23.2	85.3	72.2	55.9	

For the evaluation, we adopt the evaluation protocol of prior work [13, 38]. While it generates class-agnostic clusters, we use the Hungarian matching algorithm to find the optimal one-to-one mapping between our predictions and the ground-truth classes for a fair evaluation.

Datasets and Metrics We evaluate our framework on four diverse and challenging benchmarks: (1) COCO-Stuff [2] which has detailed pixel-level annotations, facilitating comprehensive various object understanding, we evaluate on the 27 mid-level categories; (2) Cityscapes [7], we evaluate on the 27 foreground classes, which is a common setup used in recent unsupervised segmentation literature for comprehensive scene parsing; (3) Potsdam [10] originally consisting of 6 classes, is merged into 3 distinct super-categories for this task: "Buildings", "Vegetation" (merging "Tree" and "Low veg."), and "Ground" (merging "Impervious surfaces", "Car", and "Clutter"); and (4) Pascal VOC 2012 [9], we evaluate on all 21 classes, which includes the 20 object categories plus the "background" class. For qualitative evaluation, we adopt mean intersection over union (mIoU) and pixel accuracy (Acc) as metrics, following most researches on semantic segmentation.

4.2. Quantitative Analysis

We present a comprehensive comparison of our GASeg framework, against the leading SOTA meth-

ods in self-supervised semantic segmentation. The quantitative results, presented in Table 1, demonstrate that our method achieves a new SOTA performance across all four challenging benchmarks on both metric.

Analyzing the ViT-S/8 results, on the COCO-Stuff-27, our 28.9 mIoU surpasses the previous best method, EAGLE (27.2 mIoU). This lead is also on Cityscapes, where our 21.5 mIoU represents a +1.8 mIoU leap over the next best competitor, EAGLE (19.7 mIoU). Similarly, on PASCAL VOC, we achieve 54.9 mIoU, decisively outperforming all prior work, including the strong ACSeg (47.1 mIoU) and MaskDistill (48.9 mIoU) baselines. Furthermore, our performance on the Potsdam dataset achieves 67.3 mIoU, outperforms the next best reported competitor, PriMaPs (38.9 mIoU), by an +28.4 mIoU. Given that Potsdam is dominated by geometrically-defined structures (e.g., buildings, roads) where semantic color cues are often unreliable, this significant margin strongly validates that our model's success is directly attributable to its explicit modeling of geometric and appearance priors.

We also evaluate the performance on larger ViT backbone, ViT-B/8, which also achieves top-tier mIoU results across all datasets, including 30.1 mIoU on COCO-Stuff, 23.2 mIoU on Cityscapes, and 72.2 mIoU on Potsdam. Across two different backbones and four diverse datasets, our framework consistently raises the bar for self-supervised segmentation.

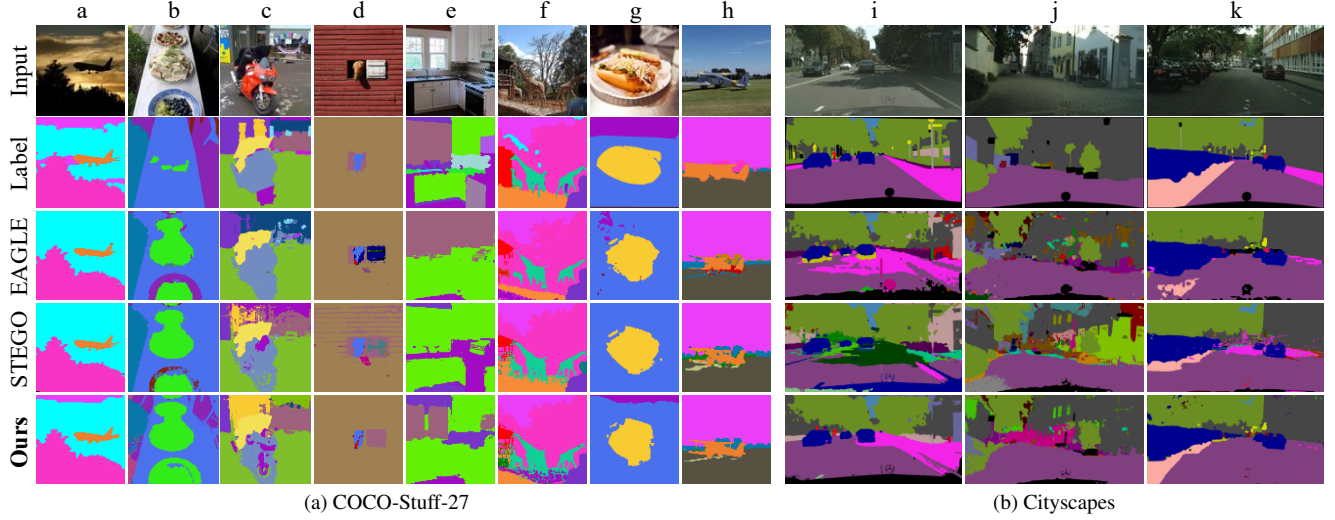


Figure 3. Qualitative semantic segmentation comparisons on the (a) COCO-Stuff-27 [2] (a - h) and (b) Cityscapes [7] (i - k) datasets. GASEg consistently produces more spatially coherent and accurate masks compared to STEGO and EAGLE.

4.3. Qualitative Analysis

Beyond the quantitative gains demonstrated in Section 4.2, we provide qualitative comparisons in Figure 3 to visually demonstrate our framework’s superiority over the leading baselines, EAGLE [20] and STEGO [13].

Across a variety of challenging scenes from COCO-Stuff 27, our method (**Ours**) produces segmentation masks that are more coherent and spatially precise to the ground truth labels (**Label**). This is particularly evident in the “Red Wall” (Figure 3a-d), where both STEGO and EAGLE produce noisy, striped artifacts, failing to capture the object’s simple, unified structure. In stark contrast, our model, guided by its geometric priors, correctly perceives this as a single, coherent surface, matching the ground truth perfectly. Furthermore, the baselines frequently fail to separate distinct adjacent objects, such as merging the “accessories” and “bicycle” (Figure 3a-c) or the “cooktop” and “cabinet” (Figure 3a-e) into single, incorrect semantic blobs.

This robust performance extends to complex street scenes, as seen in the Cityscapes examples, where our model demonstrates a clear superiority in parsing complex structures. This is especially clear in the Figure 3b-j, where STEGO and EAGLE completely fail to capture the building’s facade, shattering it into multiple spurious regions and hallucinating a “sky” class. Our model, in contrast, correctly identifies the entire “building” as a single, unified object. Furthermore, both baselines fail to delineate key boundaries, merging the “car” with the “road” (Figure 3b-k) or the “sidewalk” with the “building” (Figure 3b-i), while our method preserves these critical delineations.

This strong visual evidence confirms that our quantitative mIoU lead is the direct result of a fundamentally more

robust approach that successfully bridges volatile appearance with stable geometric structure.

4.4. Efficiency Analysis

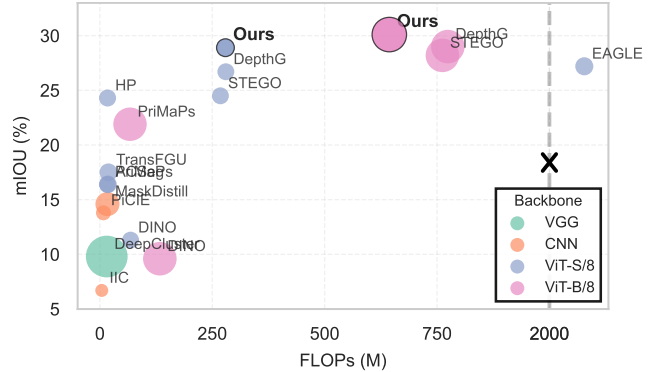


Figure 4. Efficiency analysis plotting model accuracy mIoU on COCO-Stuff against computational cost. The size of each bubble corresponds to the model’s parameter count. Our models (Ours, ViT-S/8, and ViT-B/8) establish a new SOTA efficiency frontier, achieving higher accuracy for their respective computational brackets.

We analyze the computational cost of our framework to demonstrate that our SOTA accuracy does not come at the cost of practical efficiency. Figure 4 provides a comprehensive overview of this trade-off, plotting the mIoU (%) on COCO-Stuff-27 against the inference-time FLOPs (M) for our method and all other methods analyzed in Section 4.2. This visualization clearly shows that both Ours (ViT-S/8) and Ours (ViT-B/8) establishes a new frontier for this task.

4.5. Ablation Study

To validate our framework and isolate the contribution of each component, we conduct a series of detailed ablation studies. All ablation experiments are conducted on the challenging COCO-Stuff-27 benchmark, using the DINO-pretrained ViT-S/8 backbone, reporting the standard Acc and mIoU metric.

Table 2. Ablation study on the core components, evaluated on COCO-Stuff. The upper section validates the optimal placement of TopoAug. The lower section demonstrates that all four topological descriptors in the DBC module, Semantic Area (SA), Semantic Boundary (SB), Depth Area (DA), and Depth Boundary (DB).

TopoAug	Box-Counting				Acc	mIoU
	SA	SB	DA	DB		
tea	✓	✓	✓	✓	65.1	27.1
both	✓	✓	✓	✓	66.3	27.9
stu	✓	✓	✓	✓	66.5	28.9
stu		✓	✓	✓	66.0	28.6
stu	✓		✓	✓	66.1	28.4
stu	✓	✓		✓	65.7	28.2
stu	✓	✓	✓		65.9	28.1

We first validate the placement of TopoAug and design of DBC module, with results presented in Table 2. "tea", "both", and "stu" denote applying TopoAug to only the teacher, both teacher and student, and only the student network, respectively. For the TopoAug, the first three rows of Table 2 confirms that TopoAug act as an adversarial augmentation for the student to create a crucial information gap, forcing it to learn robust features. Using the "stu" placement, achieves 28.9 mIoU, while changing this placement to "tea" or "both" causes a performance collapse to 27.1 mIoU and 27.9 mIoU, respectively.

Next, for the internal design of the DBC Module, which is built on four topological descriptors: Semantic Area (SA), Semantic Boundary (SB), Depth Area (DA), and Depth Boundary (DB). Starting from our Full Model (28.9 mIoU), we ablate each of these as shown in the last five rows of Table 2, removing any single component results in a performance drop, confirming they are all necessary.

Table 3. Ablation study on the individual components of the multi-objective GALoss function.

Exp.	\mathcal{L}_{con}	$\mathcal{L}_{\text{dist}}$	$\mathcal{L}_{\text{align}}$	\mathcal{L}_{ref}	Acc	mIoU
A	✓				53.1	20.4
B	✓	✓			57.3	22.8
C	✓	✓	✓		63.2	26.4
D	✓	✓	✓	✓	66.5	28.9

Second, we quantify the performance gain from each component of our multi-objective loss function, presented

in Table 3. We establish a minimal baseline (A) trained only with the contrastive loss \mathcal{L}_{con} , yielding 20.4 mIoU. By adding the distillation loss $\mathcal{L}_{\text{dist}}$ (B), which compares the prototypical cluster outputs of both pathways, the performance improves by +2.4 mIoU. Then, we add the cross-modal alignment loss $\mathcal{L}_{\text{align}}$ (C), which aligns the DBC module's semantic f_{sem} and geometric f_{geo} features, causes a substantial performance leap of +3.6 mIoU. Finally, our Full Model (D) adds the refinement loss \mathcal{L}_{ref} , provides a +2.5 mIoU boost to reach our final SOTA performance of 28.9 mIoU.

Table 4. Backbone generalizability analysis against SOTA, including ResNet-152, ConvNeXt, MAE, and DINO.

Backbone	Baseline		Our Framework	
	Acc	mIoU	Acc	mIoU
ResNet152 [14]	9.8	3.1	12.7	6.2
ConvNeXt [25]	14.1	8.2	19.4	9.2
SwinViT [24]	16.7	9.7	24.4	14.2
MAE [15]	17.4	10.1	30.6	16.1
DINO [32]	28.7	11.3	66.5	28.9

Finally, we validate the "backbone-agnostic" nature of our framework by applying different frozen image encoder in our framework. We build the baseline using a basic teacher-student training framework (using different augmentation strategies on each branch, no additional modules). The results are shown in Table 4. Our framework consistently provides performance lift over the baseline across all tested models. This holds true for different architectures, where our framework improves classic models like ResNet152 (+3.1 mIoU) and modern ConvNeXt (+1.0 mIoU) backbones. Crucially, our method demonstrates a massive +17.6 mIoU gain on the correspondence-based DINO and a +6.0 mIoU gain on the reconstruction-based MAE. The results confirm our framework is a general-purpose feature distillation and regularization strategy.

5. Conclusion

In this paper, we identified that topological information has been overlooked in self-supervised semantic segmentation. Motivated by this, we propose GASEG, which bridges geometric and appearance. GASEG contains a Differentiable Box-Counting module to quantify multi-scale topological statistics; a Topological Augmentation to enforce robust feature learning; and a GALoss to align these cross-modal representations. Extensive experiments show GASEG achieves state-of-the-art performance on four benchmarks. Our results validate that bridging geometry and appearance provides a more robust and accurate semantic segmentation, underscoring the potential of topological invariants for visual understanding.

References

[1] Alexander H Berger, Laurin Lux, Nico Stucki, Vincent Bürgin, Suprosanna Shit, Anna Banaszak, Daniel Rueckert, Ulrich Bauer, and Johannes C Paetzold. Topologically faithful multi-class segmentation in medical images. In *International Conference on Medical Image Computing and Computer-Assisted Intervention*, pages 721–731. Springer, 2024. [2](#)

[2] Holger Caesar, Jasper Uijlings, and Vittorio Ferrari. Coco-stuff: Thing and stuff classes in context. In *Computer vision and pattern recognition (CVPR), 2018 IEEE conference on*. IEEE, 2018. [6](#), [7](#)

[3] Luca Caltagirone, Mauro Bellone, Lennart Svensson, Matthias Wahde, and Raivo Sell. Lidar–camera semi-supervised learning for semantic segmentation. *Sensors*, 21(14):4813, 2021. [1](#)

[4] Mathilde Caron, Piotr Bojanowski, Armand Joulin, and Matthijs Douze. Deep clustering for unsupervised learning of visual features. In *Proceedings of the European conference on computer vision (ECCV)*, pages 132–149, 2018. [6](#)

[5] Mathilde Caron, Hugo Touvron, Ishan Misra, Hervé Jégou, Julien Mairal, Piotr Bojanowski, and Armand Joulin. Emerging properties in self-supervised vision transformers. In *Proceedings of the IEEE/CVF international conference on computer vision*, pages 9650–9660, 2021. [2](#)

[6] Jang Hyun Cho, Utkarsh Mall, Kavita Bala, and Bharath Hariharan. Picie: Unsupervised semantic segmentation using invariance and equivariance in clustering. In *Proceedings of the IEEE/CVF conference on computer vision and pattern recognition*, pages 16794–16804, 2021. [1](#), [6](#)

[7] Marius Cordts, Mohamed Omran, Sebastian Ramos, Timo Rehfeld, Markus Enzweiler, Rodrigo Benenson, Uwe Franke, Stefan Roth, and Bernt Schiele. The cityscapes dataset for semantic urban scene understanding. In *Proc. of the IEEE Conference on Computer Vision and Pattern Recognition (CVPR)*, 2016. [6](#), [7](#)

[8] Abhimanyu Dubey, Otkrist Gupta, Pei Guo, Ramesh Raskar, Ryan Farrell, and Nikhil Naik. Pairwise confusion for fine-grained visual classification. In *Proceedings of the European conference on computer vision (ECCV)*, pages 70–86, 2018. [1](#)

[9] Mark Everingham and John Winn. The pascal visual object classes challenge 2012 (voc2012) development kit. *Pattern Analysis, Statistical Modelling and Computational Learning, Tech. Rep*, 8(5):2–5, 2011. [6](#)

[10] International Society for Photogrammetry and Remote Sensing (ISPRS). Isprs 2d semantic labeling contest - potsdam dataset. <https://www.isprs.org/resources/datasets/benchmarks/UrbanSemLab/2d-sem-label-potsdam.aspx>. Accessed: 2025-11-10. [6](#)

[11] Yanping Fu, Wenbin Liao, Xinyuan Liu, Hang Xu, Yike Ma, Yucheng Zhang, and Feng Dai. Topologic: An interpretable pipeline for lane topology reasoning on driving scenes. *Advances in Neural Information Processing Systems*, 37:61658–61676, 2024. [2](#)

[12] Oliver Hahn, Nikita Araslanov, Simone Schaub-Meyer, and Stefan Roth. Boosting unsupervised semantic segmentation with principal mask proposals. *arXiv preprint arXiv:2404.16818*, 2024. [6](#)

[13] Mark Hamilton, Zhoutong Zhang, Bharath Hariharan, Noah Snavely, and William T Freeman. Unsupervised semantic segmentation by distilling feature correspondences. *arXiv preprint arXiv:2203.08414*, 2022. [5](#), [6](#), [7](#)

[14] Kaiming He, Xiangyu Zhang, Shaoqing Ren, and Jian Sun. Deep residual learning for image recognition. In *Proceedings of the IEEE conference on computer vision and pattern recognition*, pages 770–778, 2016. [8](#)

[15] Kaiming He, Xinlei Chen, Saining Xie, Yanghao Li, Piotr Dollár, and Ross Girshick. Masked autoencoders are scalable vision learners. In *Proceedings of the IEEE/CVF conference on computer vision and pattern recognition*, pages 16000–16009, 2022. [8](#)

[16] Wenbin He, William Surmeier, Arvind Kumar Shekar, Liang Gou, and Liu Ren. Self-supervised semantic segmentation grounded in visual concepts. In *Proceedings of the Thirty-First International Joint Conference on Artificial Intelligence, IJCAI-22*, pages 949–955. International Joint Conferences on Artificial Intelligence Organization, 2022. Main Track. [1](#)

[17] Xiaoling Hu, Fuxin Li, Dimitris Samaras, and Chao Chen. Topology-preserving deep image segmentation. *Advances in neural information processing systems*, 32, 2019. [2](#)

[18] Phillip Isola, Daniel Zoran, Dilip Krishnan, and Edward H Adelson. Learning visual groups from co-occurrences in space and time. *arXiv preprint arXiv:1511.06811*, 2015. [6](#)

[19] Xu Ji, Joao F Henriques, and Andrea Vedaldi. Invariant information clustering for unsupervised image classification and segmentation. In *Proceedings of the IEEE/CVF international conference on computer vision*, pages 9865–9874, 2019. [6](#)

[20] Chanyoung Kim, Woojung Han, Dayun Ju, and Seong Jae Hwang. Eagle: Eigen aggregation learning for object-centric unsupervised semantic segmentation. In *Proceedings of the IEEE/CVF Conference on Computer Vision and Pattern Recognition*, pages 3523–3533, 2024. [2](#), [5](#), [6](#), [7](#)

[21] Junho Kim, Byung-Kwan Lee, and Yong Man Ro. Causal unsupervised semantic segmentation. *arXiv preprint arXiv:2310.07379*, 2023. [2](#)

[22] Kehan Li, Zhennan Wang, Zesen Cheng, Runyi Yu, Yian Zhao, Guoli Song, Chang Liu, Li Yuan, and Jie Chen. Acseg: Adaptive conceptualization for unsupervised semantic segmentation. In *Proceedings of the IEEE/CVF conference on computer vision and pattern recognition*, pages 7162–7172, 2023. [2](#), [6](#)

[23] Weiquan Liu, Hanyun Guo, Weinan Zhang, Yu Zang, Cheng Wang, and Jonathan Li. Toposeg: Topology-aware segmentation for point clouds. In *Proceedings of the Thirty-First International Joint Conference on Artificial Intelligence, IJCAI-22*, pages 1201–1208. International Joint Conferences on Artificial Intelligence Organization, 2022. Main Track. [2](#)

[24] Ze Liu, Han Hu, Yutong Lin, Zhuliang Yao, Zhenda Xie, Yixuan Wei, Jia Ning, Yue Cao, Zheng Zhang, Li Dong, Furu Wei, and Baining Guo. Swin transformer v2: Scaling

up capacity and resolution. In *International Conference on Computer Vision and Pattern Recognition (CVPR)*, 2022. 8

[25] Zhuang Liu, Hanzi Mao, Chao-Yuan Wu, Christoph Feichtenhofer, Trevor Darrell, and Saining Xie. A convnet for the 2020s. In *Proceedings of the IEEE/CVF conference on computer vision and pattern recognition*, pages 11976–11986, 2022. 8

[26] Edgar Lobaton, Ram Vasudevan, Ron Alterovitz, and Ruzena Bajcsy. Robust topological features for deformation invariant image matching. In *2011 International Conference on Computer Vision*, pages 2516–2523. IEEE, 2011. 1

[27] Karim Mahrouse, Janine Bennett, Gerik Scheuermann, Bernd Hamann, and Kenneth I Joy. Topological segmentation in three-dimensional vector fields. *IEEE Transactions on Visualization and Computer Graphics*, 10(2):198–205, 2004. 2

[28] Christian Mayr, Christian Kubler, Norbert Haala, and Michael Teutsch. Narrowing the synthetic-to-real gap for thermal infrared semantic image segmentation using diffusion-based conditional image synthesis. In *Proceedings of the IEEE/CVF Conference on Computer Vision and Pattern Recognition*, pages 3131–3141, 2024. 1

[29] Fausto Milletari, Nassir Navab, and Seyed-Ahmad Ahmadi. V-net: Fully convolutional neural networks for volumetric medical image segmentation. In *2016 fourth international conference on 3D vision (3DV)*, pages 565–571. Ieee, 2016. 5

[30] Dantong Niu, Xudong Wang, Xinyang Han, Long Lian, Roei Herzig, and Trevor Darrell. Unsupervised universal image segmentation. In *Proceedings of the IEEE/CVF Conference on Computer Vision and Pattern Recognition*, pages 22744–22754, 2024. 2

[31] Aaron van den Oord, Yazhe Li, and Oriol Vinyals. Representation learning with contrastive predictive coding. *arXiv preprint arXiv:1807.03748*, 2018. 5

[32] Maxime Oquab, Timothée Darzet, Theo Moutakanni, Huy V. Vo, Marc Szafraniec, Vasil Khalidov, Pierre Fernandez, Daniel Haziza, Francisco Massa, Alaaeldin El-Nouby, Russell Howes, Po-Yao Huang, Hu Xu, Vasu Sharma, Shang-Wen Li, Wojciech Galuba, Mike Rabbat, Mido Assran, Nicolas Ballas, Gabriel Synnaeve, Ishan Misra, Herve Jegou, Julien Mairal, Patrick Labatut, Armand Joulin, and Piotr Bojanowski. Dinov2: Learning robust visual features without supervision, 2023. 5, 6, 8

[33] Maximilian Seitzer, Max Horn, Andrii Zadaianchuk, Dominik Zietlow, Tianjun Xiao, Carl-Johann Simon-Gabriel, Tong He, Zheng Zhang, Bernhard Schölkopf, Thomas Brox, et al. Bridging the gap to real-world object-centric learning. *arXiv preprint arXiv:2209.14860*, 2022. 2

[34] Hyun Seok Seong, WonJun Moon, SuBeen Lee, and Jae-Pil Heo. Leveraging hidden positives for unsupervised semantic segmentation. In *Proceedings of the IEEE/CVF conference on computer vision and pattern recognition*, pages 19540–19549, 2023. 6

[35] Hyun Seok Seong, WonJun Moon, SuBeen Lee, and Jae-Pil Heo. Leveraging hidden positives for unsupervised semantic segmentation. In *Proceedings of the IEEE/CVF conference on computer vision and pattern recognition*, pages 19540–19549, 2023. 2

[36] Hailan Shen, Zheng Tang, Yajing Li, Xuanchu Duan, and Zailiang Chen. Haic-net: Semi-supervised octa vessel segmentation with self-supervised pretext task and dual consistency training. *Pattern Recognition*, 151:110429, 2024. 2

[37] Chenbo Shi, Kang Wang, Guodong Zhang, Zelong Li, and Changsheng Zhu. Efficient and accurate semi-supervised semantic segmentation for industrial surface defects. *Scientific Reports*, 14(1):21874, 2024. 1

[38] Leon Sick, Dominik Engel, Pedro Hermosilla, and Timo Ropinski. Unsupervised semantic segmentation through depth-guided feature correlation and sampling. In *Proceedings of the IEEE/CVF Conference on Computer Vision and Pattern Recognition*, pages 3637–3646, 2024. 1, 6

[39] Shanqian Sun, Yunjia Huang, Kohei Inoue, and Kenji Hara. Order space-based morphology for color image processing. *Journal of Imaging*, 9(7):139, 2023. 5

[40] Wouter Van Gansbeke, Simon Vandenhende, and Luc Van Gool. Discovering object masks with transformers for unsupervised semantic segmentation. *arXiv preprint arXiv:2206.06363*, 2022. 6

[41] Antonin Vobecky, David Hurich, Oriane Siméoni, Spyros Gidaris, Andrei Bursuc, Patrick Pérez, and Josef Sivic. Drive&segment: Unsupervised semantic segmentation of urban scenes via cross-modal distillation. In *European conference on computer vision*, pages 478–495. Springer, 2022. 1

[42] Puyang Wang, Dazhou Guo, Dandan Zheng, Minghui Zhang, Haogang Yu, Xin Sun, Jia Ge, Yun Gu, Le Lu, Xianhua Ye, and Dakai Jin. Accurate airway tree segmentation in ct scans via anatomy-aware multi-class segmentation and topology-guided iterative learning. *IEEE Transactions on Medical Imaging*, 43(12):4294–4306, 2024. 2

[43] Qian Wu, Yufei Chen, Wei Liu, Xiaodong Yue, and Xiahai Zhuang. Deep closing: Enhancing topological connectivity in medical tubular segmentation. *IEEE Transactions on Medical Imaging*, 43(11):3990–4003, 2024. 2

[44] Zhuofan Xia, Xuran Pan, Shiji Song, Li Erran Li, and Gao Huang. Vision transformer with deformable attention. In *Proceedings of the IEEE/CVF conference on computer vision and pattern recognition*, pages 4794–4803, 2022. 4

[45] Meilong Xu, Xiaoling Hu, Saumya Gupta, Shahira Abousamra, and Chao Chen. Semi-supervised segmentation of histopathology images with noise-aware topological consistency. In *European Conference on Computer Vision*, pages 271–289. Springer, 2024. 2

[46] Lihe Yang, Bingyi Kang, Zilong Huang, Zhen Zhao, Xiaogang Xu, Jiashi Feng, and Hengshuang Zhao. Depth anything v2. *arXiv:2406.09414*, 2024. 5

[47] Lisha Yao, Yingda Xia, Zhihong Chen, Suyun Li, Jiawen Yao, Dakai Jin, Yanting Liang, Jiatai Lin, Bingchao Zhao, Chu Han, Le Lu, Ling Zhang, Zaiyi Liu, and Xin Chen. A colorectal coordinate-driven method for colorectal and colorectal cancer segmentation in conventional ct scans. *IEEE Transactions on Neural Networks and Learning Systems*, 36(4):7395–7406, 2025. 2

- [48] Zhaoyuan Yin, Pichao Wang, Fan Wang, Xianzhe Xu, Hanling Zhang, Hao Li, and Rong Jin. Transfgu: a top-down approach to fine-grained unsupervised semantic segmentation. In *European conference on computer vision*, pages 73–89. Springer, 2022. [6](#)
- [49] Feng Zhang, Xinran Liu, Changxin Gao, and Nong Sang. Color and luminance separated enhancement for low-light images with brightness guidance. *Sensors*, 24(9):2711, 2024. [5](#)
- [50] Wenbo Zhang and Achuan Wang. Research on semantic segmentation method of remote sensing image based on self-supervised learning. *International Journal of Advanced Computer Science and Applications*, 14(8), 2023. [1](#)